Inorg. Chem. **2008**, *47*, 4077−4087

A Two-Dimensional Iron(II) Carboxylate Linear Chain Polymer that Exhibits a Metamagnetic Spin-Canted Antiferromagnetic to Single-Chain Magnetic Transition

Yan-Zhen Zheng,[†] Wei Xue,[†] Ming-Liang Tong,*[,†] Xiao-Ming Chen,*[,†] Fernande Grandjean,[‡] and Gary J. Long*[,§]

MOE Laboratory of Bioinorganic and Synthetic Chemistry, School of Chemistry and Chemical Engineering, Sun Yat-Sen University, Guangzhou 510275, China, Department of Physics, B5, University of Liège, B-4000 Sart-Tilman, Belgium, and Department of Chemistry, Missouri University of Science and Technology, University of Missouri, Rolla, Missouri 65409-0010

Received September 21, 2007

A two-dimensional iron(II) carboxylate coordination polymer, $[Fe(pyoa)_2]_\infty$, where pyoa is 2-(pyridin-3-yloxy)acetate, has been prepared by hydrothermal synthesis. Its crystal structure reveals a single iron(II) site with an elongated octahedral coordination environment containing four equatorial carboxylate oxygens and two axial pyridyl nitrogens; the iron(II) sites are linked by syn−anti μ-carboxylates to form chains along the *b* axis that have an Fe···Fe separation of 4.910 Å. The shortest interchain and interlayer Fe···Fe distances are 6.453 and 11.125 Å, respectively. The 4.2−295 K Mössbauer spectra of $[Fe(pyoa)_2]_\infty$ consist of a single paramagnetic high-spin iron(II) quadrupole doublet. The axial Fe−N bond direction defines the Jahn–Teller axis at an iron(II) site and, consequently, the orientation of the single-ion magnetic anisotropy. Thus, along the *b* axis in a given chain, the spins are collinear and parallel to the Jahn–Teller axis. The Jahn–Teller axes of adjacent intralayer chains have different orientations with an angle of 79.2° between the axes in adjacent chains in a *bc* layer. $[Fe(pyoa)_2]_\infty$ exhibits field-induced metamagnetic behavior such that, in an applied field smaller than the critical field, the iron(II) spin-canted moments experience intrachain ferromagnetic interactions and weak interchain antiferromagnetic interactions; the spin canting yields weak ferromagnetism. In an applied field larger than the critical field, the weak antiferromagnetic interchain interactions are overwhelmed to yield superparamagnetic-like slow-magnetic relaxation with an energy barrier of 23(3) K. Single-crystal magnetic studies reveal a quasi-uniaxial magnetic anisotropy with the *a* axis as the easy-magnetic axis and the *b* axis as the hard-magnetic axis; the susceptibility measured along the easy *a* axis may be fit with the Glauber model to yield an effective intrachain exchange coupling constant of 2.06(8) K. A dynamic analysis of the susceptibility yields a 6.3(1) K energy barrier for intrachain domain wall creation. The observed field-assisted superparamagnet-like behavior is consistent with the dynamics of a single-chain magnet. Thus, $[Fe(pyoa)_2]_\infty$ is best considered as a "metamagnetic-like" single-chain magnet.

Introduction

There have been many recent reports[1−3] dealing with the synthesis of new one-dimensional single-chain molecular magnets in which the magnetization results from slow magnetic relaxation along the chain, relaxation that has been modeled by using the dynamic model of Glauber.[4] At low temperatures, an anisotropic Heisenberg chain, that is, an Ising chain with single-ion anisotropy, D, has magnetic domains of length 2ζ that are separated by very sharp domain walls when $|D| \gg (4/3)J_I$, where $J_I$is the intrachain exchange interaction. Further, in such chains, the magnetic correlation length, ζ, will increase exponentially with the inverse of the temperature. The thickness of an intrachain domain wall may

* To whom correspondence should be addressed. E-mail: tongml@mail.sysu.edu.cn (M.-L.T.); cxm@mail.sysu.edu.cn (X.-M.C.); glong@mst.edu (G.J.L.). Fax: (573) 341-6033 (X.-M.C.). Sun Yat-Sen University fax: (+)86 20 8411-2245 (X.-M.C.).
† Sun Yat-Sen University.
‡ University of Liège.
§ University of Missouri.

(1) For a review see: Coulon, C.; Miyasaka, H.; Clérac, R. *Struct. Bonding (Berlin)* **2006**, *122*, 163–206.

10.1021/ic701879y CCC: $40.75
Published on Web 04/19/2008

be as small as a single unit cell along the chain, that is, the length of a spin unit along the chain. The energy, Δ_ζ, needed to create such a domain wall is $4|J_I|S^2$, where S is the spin associated with the metal ions found in the chain.[1] Quasi-Ising ferromagnetic chains, that is, chains with a helical arrangement of the local anisotropy tensors, may easily lead to large oriented domain walls.[1,2a,i] Although such large domain walls do not affect the Glauber dynamics,[4] the local anisotropy tensors of the spins should have the same orientation in order to yield single-chain magnetic systems that qualify as being in the "Ising limit" for which $|D| \gg (4/3)J_I$.

The control of the ratio of intrachain to interchain magnetic interactions is another key factor in designing a single-chain molecular magnet. Such control is important because three-dimensional magnetic order often competes with one-dimensional order, particularly at low temperatures, as the chain magnetic domains of length 2ζ become very large.[1] As a consequence, many chain compounds exhibiting three-dimensional magnetic ordering have been reported, even though their interchain magnetic interactions are small.[5,6]

In the special case of weak antiferromagnetic interchain interactions, metamagnetic behavior may be observed if an applied magnetic field overwhelms the weak interchain interactions and, as a consequence, there is a crossover from one magnetic ground state to another.[7–11] Most previously investigated[7,8] one-dimensional metamagnets exhibit a crossover from an antiferromagnetic or paramagnetic state to a ferromagnetic three-dimensional state; only a few[9,10a,b] exhibit slow magnetic relaxation, and the latter are interesting because they can be regarded as intermediates between classical three-dimensional magnets and single-chain magnets. Their properties have been described as exhibiting "metamagnetic-like single-chain magnetic" behavior,[9a,b] behavior that has many potential applications including future high-density information storage.[1,12]

There typically are only two methods by which such chains may be synthesized. One method, the "bottom-up" or "step-by-step" method, requires preformed magnetic units that are then "strung together" with appropriate bridging ligands.[2b–h,13] The second method, the "one-pot" method, combines all the necessary components into one reaction.[2a,i–q,3] The former method seems more "rational" than the latter and also yields some unexpected high-dimensional compounds, which provide

(2) (a) Co^{II}_{oct}−radical: Caneschi, A.; Gatteschi, D.; Lalioti, N.; Sangregorio, C.; Sessoli, R.; Venturi, G.; Vindigni, A.; Rettori, A.; Pini, M. G.; Novak, M. A. *Angew. Chem., Int. Ed.* **2001**, *40*, 1760–1763. (b) Ni^{II}−Mn^{III}: Clérac, R.; Miyasaka, H.; Yamashita, M.; Coulon, C. *J. Am. Chem. Soc.* **2002**, *124*, 12837–12844. (c) Co^{II}_{oct}−Fe^{III}: Lescouëzec, R.; Vaissermann, J.; Ruiz-Pérez, C.; Lloret, F.; Carrasco, R.; Julve, M.; Verdaguer, M.; Draomzee, Y.; Gatteschi, D.; Wernsdorfer, W. *Angew. Chem., Int. Ed.* **2003**, *42*, 1483–1486. (d) Fe^{III}−Cu^{II}: Wang, S.; Zuo, J.-L.; Gao, S.; Zhou, H.-C.; Zhang, Y.-Z.; You, X.-Z. *J. Am. Chem. Soc.* **2004**, *126*, 8900–8901. (e) Co^{II}_{oct}−Cu^{II}: Pardo, E.; Ruiz-Garcia, R.; Lloret, F.; Faus, J.; Julve, M.; Journaux, Y.; Delgado, F.; Ruiz-Pérez, C. *Adv. Mater.* **2004**, *16*, 1597–1600. (f) Fe^{III}−Mn^{III}: Ferbinteanu, M; Marilena, H.; Wernsdorfer, W.; Nakata, K.; Sugiura, K.-I.; Yamashita, M.; Coulon, C.; Clérac, R. *J. Am. Chem. Soc.* **2005**, *127*, 3090–3099. (g) Fe^{II}−Fe^{III}: Kajiwara, T.; Nakano, M.; Kaneko, Y.; Takaishi, S.; Ito, T.; Yamashita, M.; Igashira-Kamiyama, A.; Nojiri, H.; Ono, Y.; Kojima, N. *J. Am. Chem. Soc.* **2005**, *127*, 10150–10151. (h) Co^{II}_{oct}−Fe^{III}: Toma, L. M.; Lescouëzec, R.; Pasán, J.; Ruiz-Pérez, C.; Vaissermann, J.; Cano, J.; Carrasco, R.; Wernsdorfer, W.; Lloret, F.; Julve, M. *J. Am. Chem. Soc.* **2006**, *128*, 4842–4853. (i) Homo−Co^{II}_{oct}: Liu, T.-F.; Fu, D.; Gao, S.; Zhang, Y.-Z.; Sun, H.-L.; Su, G.; Liu, Y.-J. *J. Am. Chem. Soc.* **2003**, *125*, 13976–13977. (j) Mn^{III}−Mn^{IV}: Chakov, N. E.; Wernsdorfer, W.; Abboud, K. A.; Christou, G. *Inorg. Chem.* **2004**, *43*, 5919–5930. (k) Cu^{II}−Ln^{III}: Costes, J.-P.; Clemente-Juan, J. M.; Dahan, F.; Milon, J. *Inorg. Chem.* **2004**, *43*, 8200–8202. (l) Mn^{II}−Mn^{III}: Shaikh, N.; Panja, A.; Goswami, S.; Banerjee, P.; Vojtisek, P.; Zhang, Y.-Z.; Su, G.; Gao, S. *Inorg. Chem.* **2004**, *43*, 849–851. (m) Dy^{III}−radical: Bogani, L.; Sangregorio, C.; Sessoli, R.; Gatteschi, D. *Angew. Chem., Int. Ed.* **2005**, *44*, 5817–5821. (n) Co^{II}_{oct}: Sun, Z.-M.; Prosvirin, A. V.; Zhao, H.-H.; Mao, J.-G.; Dunbar, K. R. *J. Appl. Phys.* **2005**, 97. (o) Mn^{III}−radical: Miyasaka, H.; Madanbashi, T.; Sugimoto, K.; Nakazawa, Y.; Wernsdorfer, W.; Sugiura, K.-I.; Yamashita, M.; Coulon, C.; Clérac, R. *Chem.*−*Eur. J.* **2006**, *12*, 7028–7040. (p) Homo−Mn^{III}: Bai, Y.-L.; Tao, J.; Wernsdorfer, W.; Sato, O.; Huang, R.-B.; Zheng, L.-S. *J. Am. Chem. Soc.* **2006**, *128*, 16428–16429. (q) Homo−Ni^{II}: Liu, X.-T.; Wang, X.-Y.; Zhang, W.-X.; Cui, P.; Gao, S. *Adv. Mater.* **2006**, *18*, 2852–2856. (r) Homo−Mn^{III}: Xu, H.-B.; Wang, B.-W.; Pan, F.; Wang, Z.-M.; Gao, S. *Angew. Chem., Int. Ed.* **2007**, *46*, 7388–7392; oct = octahedral.

(3) (a) Homo−Co^{II}_{sq}: Zheng, Y.-Z.; Tong, M.-L.; Zhang, W.-X.; Chen, X.-M. *Angew. Chem., Int. Ed.* **2006**, *45*, 6310–6314. (b) Homo−Co^{II}_{oct}: Cheng, X.-N.; Zhang, W.-X.; Zheng, Y.-Z.; Chen, X.-M. *Chem. Commun.* **2006**, 3603–3605. (c) Mixed Co^{II}_{oct} and Co^{II}_{tbp}: Li, X.-J.; Wang, X.-Y.; Gao, S.; Cao, R. *Inorg. Chem.* **2006**, *45*, 1508–1516; oct = octahedral, sq = square pyramidal and tbp = trigonal bipyramidal.

(4) Glauber, R. J. *J. Math. Phys.* **1963**, *4*, 294–307.

(5) For a review, see: Georges, R.; Borrás-Almenar, J. J.; Coronado, E.; Curély, J.; Drillon M. *One-dimensional Magnetism: An Overview of the Models in Magnetism: Molecules to Materials*; Miller, J. S., Drillon, M., Eds.; Wiley-VCH Verlag: Berlin, 2001; Vol. I, pp 1–47.

(6) (a) Kahn, O. *Molecular Magnetism*; VCH: New York, 1993. (b) Carlin, R. L. *Magnetochemistry*; Springer: Berlin, 1986.

(7) (a) Matsumoto, N.; Sunatsuki, Y; Miyasaka, H.; Hashimoto, Y.; Luneau, D.; Tuchagues, J.-P. *Angew. Chem., Int. Ed.* **1998**, *38*, 171–173. (c) Humphrey, S. M.; Wood, P. T. *J. Am. Chem. Soc.* **2004**, *126*, 13236–13237. (e) Zheng, L.-M.; Gao, S.; Yin, P.; Xin, X.-Q. *Inorg. Chem.* **2003**, *42*, 2151–2156. (f) Wang, R.; Gao, E.; Hong, M.; Gao, S.; Luo, J.; Lin, Z.; Han, L.; Cao, R. *Inorg. Chem.* **2003**, *42*, 5486–5488. (g) Chang, W.-K.; Chiang, R.-K.; Jiang, Y.-C.; Wang, S.-L.; Lee, S.-F.; Lii, K.-H. *Inorg. Chem.* **2004**, *43*, 2564–2568. (h) Ko, H. H.; Lim, J. H.; Kim, H. C.; Hong, C. S. *Inorg. Chem.* **2006**, *45*, 8847–8849. (i) Yoon, J. H.; Lim, J. H.; Choi, S. W.; Kim, H. C.; Hong, C. S. *Inorg. Chem.* **2007**, *46*, 1529–1531. (j) Bellitto, C.; Federici, F. *Inorg. Chem.* **2002**, *41*, 709–714.

(8) (a) Fu, A.; Huang, X.; Li, J.; Yuen, T.; Lin, C. L. *Chem.*−*Eur. J.* **2002**, *8*, 2239–2247. (b) Wang, X.-Y.; Wang, L.; Wang, Z.-M.; Su, G.; Gao, S. *Chem. Mater.* **2005**, *17*, 6369–6380. (c) Gao, E.-Q.; Wang, Z.-M.; Yan, C.-H. *Chem. Commun.* **2003**, 1748–1749. (d) Monfort, M.; Resino, I.; El Fallah, M. S.; Ribas, J.; Solans, X.; Font-Bardia, M.; Stoeckli-Evans, H. *Chem.*−*Eur. J.* **2001**, *7*, 280–287. (e) Liu, T.; Zhang, Y.; Wang, Z.; Gao, S. *Inorg. Chem.* **2006**, *45*, 2782–2784. (f) Liu, P.-P.; Cheng, A.-L.; Liu, N.; Sun, W.-W.; Gao, E.-Q. *Chem. Mater.* **2007**, *19*, 2724–2726.

(9) (a) Toma, L. M.; Lescouëzec, R.; Lloret, F.; Julve, M.; Vaissermann, J.; Verdaguer, M. *Chem. Commun.* **2003**, 1850–1851. (b) Toma, L. M.; Delgado, F. S.; Ruiz-Pérez, C.; Carrasco, R.; Cano, J.; Lloret, F.; Julve, M. *Dalton Trans.* **2004**, 2836–2837. (c) Pereira, C. L. M.; Pedroso, E. F.; Stumpf, H. O.; Novak, M. A.; Ricard, L.; Ruiz-García, R.; Rivière, E.; Journaux, Y. *Angew. Chem., Int. Ed.* **2004**, *43*, 956–958. (d) He, Z.; Wang, Z.-M.; Gao, S.; Yan, C.-H. *Inorg. Chem.* **2006**, *45*, 6694–6705.

(10) (a) Ma, B.-Q.; Gao, S.; Su, G.; Xu, G.-X. *Angew. Chem., Int. Ed.* **2001**, *40*, 434–437. (b) Gao, S.; Su, G.; Yi, T.; Ma, B.-Q. *Phys. Rev. B: Condens. Matter Mater. Phys.* **2001**, *63*–6. (c) Kou, H.-Z.; Gao, S.; Sun, B.-W.; Zhang, J. *Chem. Mater.* **2001**, *13*, 1432–1434. (d) Paul, G.; Choudhury, A.; Rao, C. N. R. *Chem. Mater.* **2003**, *15*, 1174–1180. (e) Zhang, Y.-Z.; Gao, S.; Sun, H.-L.; Su, G.; Wang, Z.-M.; Zhang, S.-W. *Chem. Commun.* **2004**, 1906–1907. (f) Zeng, M.-H.; Zhang, W.-X.; Sun, X.-Z.; Chen, X.-M. *Angew. Chem., Int. Ed.* **2005**, *44*, 3079–3082.

(11) (a) Yin, P.; Zheng, L.-M.; Gao, S.; Xin, X.-Q. *Chem. Commun.* **2001**, 2346–2347. (b) Liu, T.-F.; Sun, H.-L.; Gao, S.; Zhang, S.-W.; Lau, T.-C. *Inorg. Chem.* **2003**, *42*, 4792–4794.

(12) (a) For reviews, see: Christou, G.; Gatteschi, D.; Hendrickson, D. N.; Sessoli, R. *MRS Bull.* **2000**, *25*, 66–71. (b) Gatteschi, D.; Sessoli, R. *Angew. Chem., Int. Ed.* **2003**, *43*, 268–297. (c) Aromí, G.; Brechin, E. K. *Struct. Bonding (Berlin)* **2006**, *122*, 1–67.

Scheme 1. Structure of the Bifunctional pyoa Ligand

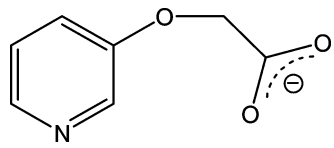

a transition between classical and quantum magnetism.[14] Our recently developed "polymerization" strategy for the preparation of single-chain magnetic compounds belongs to the second method.[3a]

In order to design viable single-chain magnetic compounds, the proper choice of ligands is an important step that must be guided both by the need for simplicity in terms of molecular structure and magnetic properties and by the affinity of the ligands for bonding into extended networks. On the basis of these requirements, we have successfully used a fully σ-bonded 1,2-cyclohexane-dicarboxylate ligand both to connect anisotropic cobalt(II) ions to form an Ising-like ferromagnetic chain and to minimize the interchain magnetic interactions.[3a,15b] Herein, we expand this investigation to a partially σ-bonded ligand, 2-(pyridin-3-yloxy)acetic acid, pyoaH (see Scheme 1), to create a new two-dimensional iron(II) coordination polymer with the $[Fe(pyoa)_2]_\infty$, **1**, stoichiometry. This new compound, which features a ferromagnetic syn−anti μ-carboxylate-bridged iron(II) chain, exhibits an unusual field-induced magnetic transition from a spin-canted antiferromagnetic state to a single-chain magnetic state.

Experimental Section

Materials and Physical Measurements. Commercially available reagents have been used as received without further purification. The C, H, and N microanalyses have been carried out with an Elementar Vario-EL CHNS elemental analyzer. The FT-IR spectra have been recorded from KBr pellets in the range 400–4000 cm^{-1} on a Bio-Rad FTS-7 spectrometer. Powder X-ray diffraction measurements have been obtained with a Rigaku D/max-IIIA diffractometer by using Cu Kα, λ = 1.540 56 Å, radiation and a scan rate of 2°/min over a 2θ range of 4−55°. A simulated X-ray diffraction pattern was generated by using the Cambridge Mercury 1.4.2 software.

The Mössbauer spectral absorber contained 18 mg/cm^2 of a finely powdered sample of **1**, and the spectra have been obtained from 4.2 to 295 K on a constant acceleration spectrometer that utilized a rhodium matrix cobalt-57 source and was calibrated at room temperature with α-iron foil. The spectra, which clearly showed the presence of texture in the absorber, have been fit with a quadrupole doublet whose isomer shift and quadrupole splitting have relative statistical errors of ca. ±0.005 and ±0.01 mm/s, respectively. The absolute errors are approximately twice as large.

Magnetic susceptibility measurements on **1** have been carried out on a Quantum Design MPMS-XL7 SQUID magnetometer between 1.8 and 300 K and ±7 T. The ac susceptibility measurements have been performed at frequencies between 1 and 1500 Hz with an ac field of 0.0005 T and with a zero or 0.1 T applied dc field. The zero-field-cooled magnetization was obtained upon warming after zero-field cooling from 300 to 1.8 K. The field-cooled magnetization was obtained upon warming after constant 0.001 and 0.1 T applied-field cooling from 300 to 1.8 K. A powder sample of **1** was embedded in grease to avoid any field-induced crystal reorientation. Single-crystal magnetic measurements were carried out by attaching a crystal to a rotator with GE7031 varnish. A diamagnetic correction of -1.8×10^{-4} emu mol^{-1} was calculated from Pascal constants and applied to the observed magnetic susceptibility of **1**.

Typical Synthetic Procedure. A mixture of iron powder (0.014 g, 0.25 mmol) and pyoaH (0.077 g, 0.5 mmol) in 17 mL of degassed water was sealed in a 23 mL Teflon-lined autoclave and heated at 140 °C for 4 days to yield yellow platelike crystals of **1** with a yield of 91%. Powder X-ray diffraction measurements verified that **1** was phase-pure, see Figure S1 of the Supporting Information. IR data for **1** (v, cm^{-1}): 3136(w), 3000(w), 1600(vs), 1484(s), 1436(s), 1413(s), 1330(m), 1277(s), 1239(s), 1189(m), 1127(m), 1062(w), 1041(m), 1019(w), 923(m), 808(m), 720(m), 697(m), 637(m), 605(m), 419(w). Anal. Calcd for $C_{14}H_{12}FeN_2O_6$: C, 46.70; H, 3.36; N, 7.78. Found: C, 46.67; H, 3.39; N, 7.75%. A 0.2 mg and 2.5 × 1.0 × 0.15 mm^3 volume single crystal of **1** for use in the single-crystal magnetic measurements was grown over 2 weeks, see Figure S2 of the Supporting Information.

X-Ray Crystallography. Single-crystal X-ray diffraction intensities of **1** were collected on a Bruker Apex CCD area-detector diffractometer by using Mo Kα (λ = 0.710 73 Å) radiation. Absorption corrections have been applied by using the multiscan program SADABS.[16] The structure was solved with direct methods and refined with a full-matrix least-squares technique using the SHELXTL program package.[17] Anisotropic thermal parameters have been assigned to all non-hydrogen atoms. The organic-ligand bound hydrogen atoms were generated geometrically at a C−H distance of 0.96 Å. Data collection and structural refinement parameters are given in Table 1, and selected bond distances and angles are given in Table 2.

Results and Discussion

Synthesis and Structural Characterization. The synthesis of **1** was achieved through a metal−carboxylic acid reaction. The oxidation of iron(II) to iron(III) during the hydrothermal synthesis was avoided by filling a Teflon-lined high-pressure vessel three-quarters with degassed water. The yellow crystals of **1** are obtained in 91% yield and are stable in the air. A large single crystal of **1** was obtained by extending the reaction time to 2 weeks. However, further

(13) (a) Miyasaka, H.; Clérac, R.; Mizushima, K.; Sugiura, K.-I.; Yamashita, M.; Wernsdorfer, W.; Coulon, C. *Inorg. Chem.* **2003**, *42*, 8203–8213. (b) Miyasaka, H.; Nezu, T.; Sugimoto, K.; Sugiura, K.-I.; Yamashita, M.; Clérac, R. *Inorg. Chem.* **2004**, *43*, 5486–5488. (c) Miyasaka, H.; Nezu, T.; Kunihisa, S.; Sugiura, K.-I.; Yamashita, M.; Clérac, R. *Chem.—Eur. J.* **2005**, *11*, 1592–1602. (d) Lecren, L.; Wernsdorfer, W.; Li, Y.-G.; Vindigni, A.; Miyasaka, H.; Clérac, R. *J. Am. Chem. Soc.* **2007**, *129*, 5045–5051. (e) Saitoh, A.; Miyasaka, H.; Yamashita, M.; Clérac, R. *J. Mater. Chem.* **2007**, *17*, 2002–2012.

(14) (a) Miyasaka, H.; Yamashita, M. *Dalton Trans.* **2007**, 399–406. (b) Miyasaka, H.; Nakata, K.; Lollita, L.; Coulon, C.; Nakazawa, Y.; Fujisaki, T.; Sugiura, K.-I.; Yamashita, M.; Clérac, R. *J. Am. Chem. Soc.* **2006**, *128*, 3770–3783. (c) Lecren, L.; Roubeau, O.; Coulon, C.; Li, Y.-G.; Goff, X. F. L.; Wernsdorfer, W.; Miyasaka, H.; Clérac, R. *J. Am. Chem. Soc.* **2005**, *127*, 17353–17363. (d) Miyasaka, H.; Nakata, K.; Sugiura, K.-I.; Yamashita, M.; Clérac, R. *Angew. Chem., Int. Ed.* **2004**, *43*, 707–711.

(15) (a) Kramer, L. S.; Clauss, A. W.; Francesconi, L. C.; Corbin, D. R.; Hendrickson, D. N.; Stucky, G. D. *Inorg. Chem.* **1981**, *20*, 2070–2077. (b) Zheng, Y.-Z.; Tong, M.-L.; Zhang, W.-X.; Chen, X.-M. *Chem. Commun.* **2006**, 165–167.

(16) Sheldrick, G. M. *SADABS 2.05*; University Göttingen: Göttingen, Germany.

(17) *SHELXTL 6.10*; Bruker Analytical Instrumentation: Madison, WI, 2000.

Table 1. Crystallographic Data and Structural Refinement for **1**

formula	$C_{14}H_{12}FeN_2O_6$
fw (g/mol)	360.11
T (K)	288 (2)
space group	$C2/c$ (No. 15)
a (Å)	21.702 (2)
b (Å)	4.9098 (4)
c (Å)	12.907 (1)
β (deg)	91.580(2)
V (Å^3)	1374.72(3)
Z	4
D_c (g cm^{-3})	1.740
μ (mm^{-1})	1.133
data collected/unique	5418/1505
R_1 ($>2\sigma$/all data)	0.0278/0.0295
wR_2 ($>2\sigma$/all data)	0.0701/0.0711
GOF	1.053
residues (e Å^{-3})	−0.245/0.291

prolonging the reaction time no longer yields single crystals, a failure that suggests a saturated equivalence between the crystal and the mother liquid.

A single-crystal X-ray diffraction indicates that **1** crystallizes in the monoclinic $C2/c$ space group. Because the iron(II) ion is located on an inversion center, the asymmetric unit, $Fe_{0.5}C_7H_6O_3N$, contains one-half of an iron(II) ion and one pyoa ligand, see Figure 1 and Figure S3 of the Supporting Information. Two adjacent iron(II) ions are related in a given chain by a translation along the b axis, see Figure 1a, and between chains by a translation along the c axis followed by a C_2 rotation about the b axis, see Figure 1b.

The iron(II) ion in **1** has an elongated octahedral coordination environment composed of four equatorial oxygens, arising from four carboxylate ligands, at Fe−O distances of 2.060(1) to 2.172(1) Å, and two strictly axial nitrogens, arising from the pyridyl ring, at an Fe−N distance of 2.279(1) Å; the N−Fe−N axis is thus the Jahn–Teller axis of the iron(II) ion. The iron(II) ions are linked by syn−anti μ-carboxylates with a separation of 4.910 Å along the b axis, see Figure 1a, forming an iron(II)−carboxylate linear spin-chain. These chains are further connected by the pyoa ligand to form a two-dimensional layer with a shortest intralayer Fe···Fe distance of 6.453 Å. It should be noted that the Jahn–Teller axes of the iron(II) ions in a given iron(II)−carboxylate chain are all parallel, see Figure 1a. However, as is shown in Figure 1b and Scheme 2, the Jahn–Teller axes of adjacent intralayer chains have different orientations with an N−Fe···Fe*−N* dihedral angle of 19.9° and an angle of 79.2° between the Fe−N and Fe*−N* vectors, where the Fe and N and Fe* and N* atoms are found in adjacent chains in a given bc layer of **1**. Further, these Jahn–Teller axes make angles of 25.75, 81.04, and 64.52° with the a, b, and c axes, respectively; that is, neither of the Jahn–Teller axes are parallel with any of the unit-cell axes. If these two sets of Jahn–Teller axes are projected onto the ab plane, the a axis is parallel with their bisector, see Scheme 2. Because the b axis is perpendicular to the ac plane, the projections of these two sets of Jahn–Teller axes onto the ac plane coincide, see Figure 1c. The adjacent layers in this figure, which are separated by $a/2$ or 10.851 Å, are stacked in an AAA fashion with a shortest Fe···Fe interlayer distance of 11.125 Å.

Bond valence sum calculations[18] with an r_0(Fe−O) value of 1.734 Å yield a mean iron valence of 1.946(2) for **1**, confirming that the iron is unambiguously divalent, a conclusion that is fully supported by the following Mössbauer spectral results.

Mössbauer Spectral Results. The Mössbauer spectra of **1** have been measured between 4.2 and 295 K and fit with a single quadrupole doublet. The resulting spectral hyperfine parameters are given in Table 3, and selected spectra are shown in Figure 2. All of the spectra are clearly indicative of high-spin iron(II) in the distorted octahedral coordination environment found in **1**; there is no indication of the presence of any iron(III) impurity. The asymmetry in the intensity of the two components of the doublet, most apparent at 295 K, arises from a platelike texture inherent in the sample. As may be observed in Figure 2, the 4.2 K spectrum is somewhat broader than the remaining spectra, a broadening that no doubt arises from the onset of long-range magnetic order in **1** just below 4.2 K.

The temperature dependence of the isomer shift results from the second-order Doppler shift. A fit of this temperature dependence yields[19] a Mössbauer temperature of 365(11) K, a value that is somewhat larger than the values of ca. 200 K typically observed in monomeric iron(II) complexes; the somewhat higher value probably results because of the polymeric nature of **1**. The maximum at ca. 85 K in the temperature dependence of the quadrupole splitting is unexpected and may result either from small changes in the coordination geometry below 85 K or from different signs and temperature dependencies of the valence and lattice contributions to the electric field gradient experienced by the iron(II) ion in **1**. The normal increase in the spectral absorption area between 295 and 4.2 K results from the increase in the recoil-free fraction upon cooling. A fit of this temperature dependence yields[19] a Mössbauer temperature, a temperature that is analogous to the Debye temperature, of 224(3) K, a value that is characteristic of an iron(II) complex. This value is lower than the value obtained from the isomer shift because the isomer shift and spectral absorption area sample different portions of the phonon spectrum.

Metamagnetic Behavior. The magnetic properties of **1** have initially been measured on a randomly oriented powder, and the 10 to 300 K dc susceptibility is shown in Figure 3. At 300 K, **1** has a χT value of 4.00 cm^3 mol^{-1} K and a corresponding effective magnetic moment, μ_{eff}, of 5.66 μ_B, values that are significantly larger than the spin-only χT of 3.00 cm^3 mol^{-1} K and the corresponding spin-only μ_{eff} of 4.90 μ_B as a result of a significant orbital contribution. Between 14 and 300 K, the magnetic susceptibility obeys the Curie–Weiss law, $\chi_M = C/(T - \Theta)$, with a Curie constant, C, of 3.91 cm^3 mol^{-1} K, a corresponding μ_{eff} of 5.59 μ_B, and a Weiss temperature, Θ, of 3.47 K. In addition to a

(18) Brown, I. D.; Altermatt, D. *Acta Crystallogr., Sect. B* **1985**, *41*, 244–247.

(19) (a) Shenoy, G. K.; Wagner, F. E.; Kalvius, G. M. In *Mössbauer Isomer Shifts*; Shenoy, G. K., Wagner, F. E., Eds.; North-Holland Publishing Company: Amsterdam, 1978; p 51. (b) Long, G. J.; *Mössbauer Spectroscopy Applied to Inorganic Chemistry*; Plenum Press: New York, 1984; Vol. 1.

Table 2. Selected Bond Lengths (Å) and Angles (deg) for **1**

Fe(1)−O(1)[a]	2.0601(11)	Fe(1)−N(1)	2.2787(14)	Fe(1)−O(2)[b]	2.1720(11)
O(1)[a]−Fe(1)−O(1)[c]	180	O(2)[b]−Fe(1)−O(2)[d]	180	O(2)[b]−Fe(1)−N(1)	94.23(5)
O(1)[a]−Fe(1)−O(2)[b]	90.84(4)	O(1)[a]−Fe(1)−N(1)	86.44(5)	O(2)[d]−Fe(1)−N(1)	85.77(5)
O(1)[c]−Fe(1)−O(2)[b]	89.16(4)	O(1)[c]−Fe(1)−N(1)	93.56(5)	N(1)[e]−Fe(1)−N(1)	180

[a] $-x+1, y-1, -z+5/2$. [b] $-x+1, y, -z+5/2$. [c] $x, -y+1, z-1/2$. [d] $x, -y, z-1/2$. [e] $-x+1, -y, -z+2$.

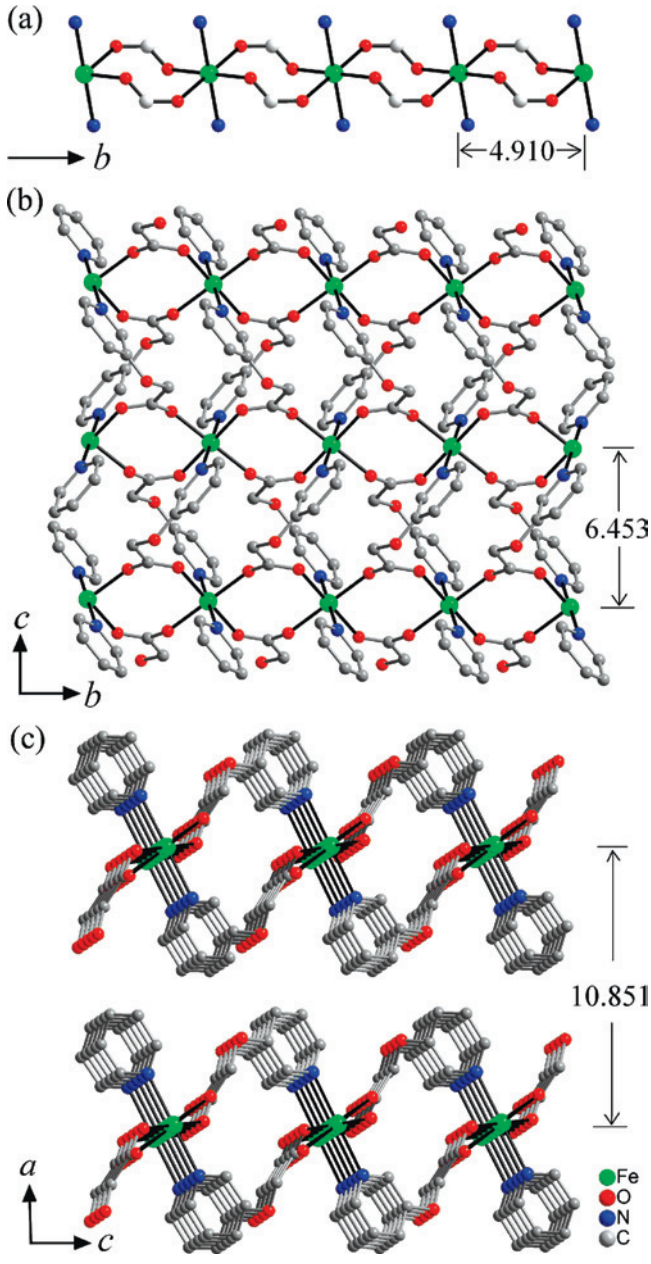

Figure 1. Perspective views of the syn−anti μ-carboxylate-bridged linear iron(II) chain (a), the pyoa-bridged layer (b), and the packing of the layers (c) in **1**. All distances are given in Ångstroms, and iron(II) is shown in green, oxygen in red, nitrogen in blue, and carbon in grey; the hydrogen atoms have been omitted.

significant orbital contribution to the moment, this Curie constant, the corresponding μ_{eff}, and the positive Θ indicate the presence of a net ferromagnetic interaction in **1**. The temperature dependence of the magnetic susceptibility of **1** above 14 K is well fit by the modified Fisher model[20] for a

(20) Fisher, M. E. *Am. J. Phys.* **1964**, *32*, 343–346.

Scheme 2. A View, in the *ab* Plane and down the *c* Axis of **1,** of the Projection of the Magnetic Moments along the Jahn−Teller Axes in an Applied Field Smaller than, Top, And Larger than, Bottom, the Critical Field, H_c[a]

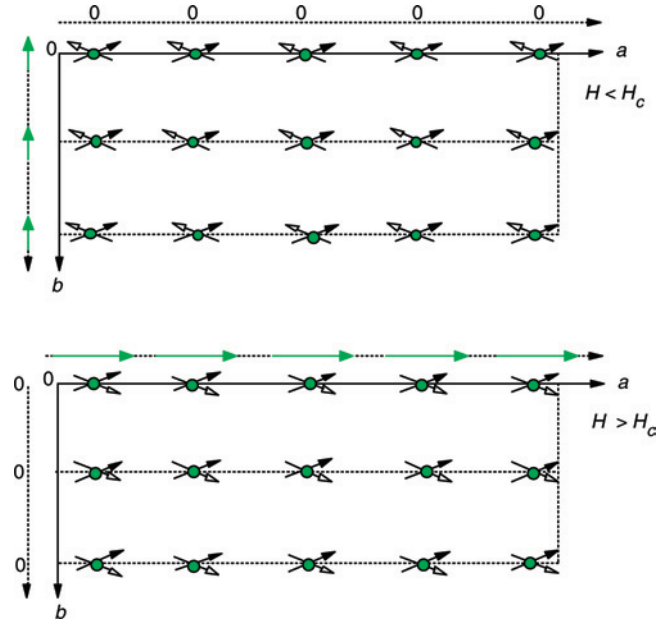

[a] The solid arrows represent one layer of moments, and the open arrows represent the next layers of moments at $\pm c/2$. The projections of these moments on the *a* axis and *b* axis are shown at the top and left of the diagram, respectively; the 0 represents a zero projected moment. Note that in both cases the *a* axis bisects the angle between the moments.

Table 3. The Mössbauer Spectral Parameters of **1**

T, K	δ, mm/s[a]	ΔE_Q, mm/s	Γ, mm/s	area, (%ϵ) (mm/s)
295	1.204	2.17	0.26	1.094
85	1.329	2.83	0.30	1.842
50	1.334	2.82	0.27	2.001
20	1.335	2.72	0.27	2.070
4.2	1.336	2.69	0.39	2.156

[a] The isomer shifts are given relative to room-temperature α-iron powder.

one-dimensional Heisenberg chain of $S = 2$ spins. The corresponding spin Hamiltonian is given by

$$\hat{H} = -J_{\text{I}} \sum_{i=1}^{N} S_i S_{i+1} + g\mu_{\text{B}} H \sum_{i=1}^{N} S_i \qquad (1)$$

where J_{I} is the intrachain coupling constant. The best fit, shown as a solid red line in Figure 3, yields $J_{\text{I}}/k_{\text{B}} = 0.80(1)$ K and $g = 2.292(1)$. An attempt to obtain the interchain interactions through the mean-field approximation was unsuccessful. The positive J_{I} value indicates that the intrachain interactions are very weakly ferromagnetic, in agreement with previously reported J values for syn−anti μ-carboxylate complexes.[11b,21] Below 14 K, the temperature dependence of the dc magnetic susceptibility was measured in several applied fields, as is shown in the inset to Figure 3. For fields smaller than 0.1 T, the maximum observed at ca. 2.5 K suggests that spontaneous antiferromagnetic

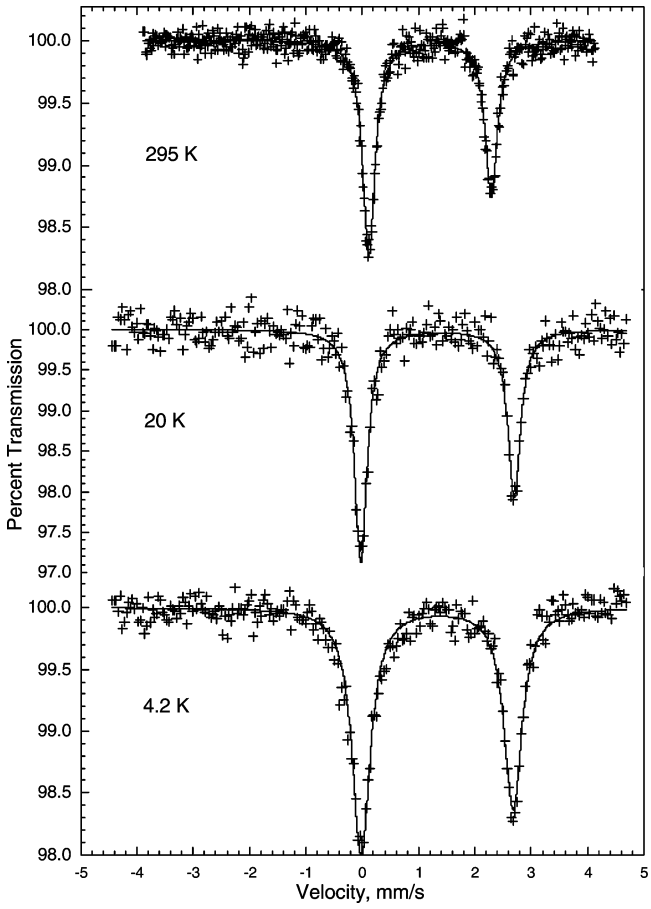

Figure 2. Mössbauer spectra of **1** obtained at the indicated temperatures.

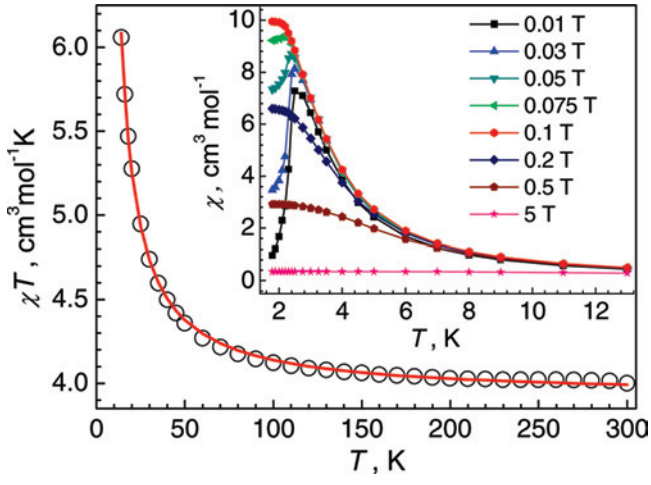

Figure 3. The temperature dependence of χT measured in an applied field of 0.1 T on a powder sample of **1**. The red line is the result of a fit between 14 and 300 K with eq 1. Inset: The temperature dependence of the magnetic susceptibility of **1** measured between 1.8 and 13 K at the indicated applied fields.

ordering of the iron(II) magnetic moments occurs between chains. For applied fields above 0.1 T, this maximum vanishes, and the susceptibility reaches a maximum at 2 K, albeit with a lower susceptibility.

The metamagnetic behavior of **1** is indicated by its isothermal magnetization behavior, see Figure 4. The slope of the small-field magnetization observed at 1.8 K is clearly different from that observed above 2 K, see the inset to

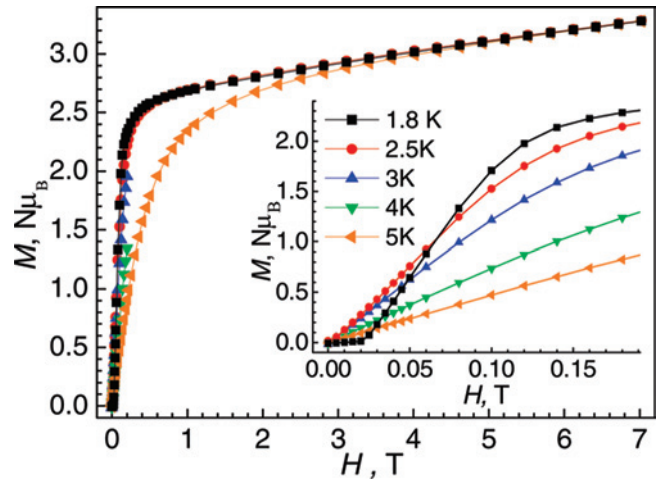

Figure 4. The field dependence of the magnetization of a powder sample of **1** obtained at the indicated temperatures. Inset: An expanded view of the magnetization obtained at small applied fields.

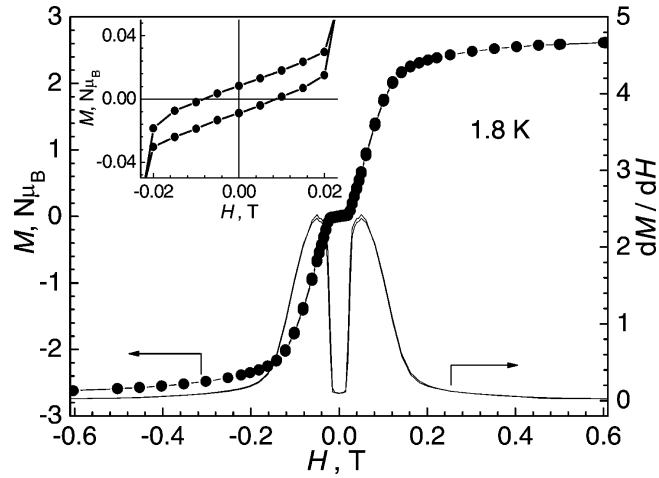

Figure 5. The magnetic hysteresis, solid points, and dM/dH, solid line, observed at 1.8 K on a powder sample of **1**. Inset: The expanded hysteresis loop obtained at small applied fields.

Figure 4. This behavior indicates a metamagnetic transition at a critical field, H_c, of 0.05(2) T, a field that is obtained from the rounded maximum observed in a plot of dM/dH as a function of applied field, see Figure 5. Below the critical field, the field dependence of the magnetization is typical of a spin-canted antiferromagnet, whereas above this field, all of the iron(II) moments are oriented parallel with the applied field. Moreover, the interchain magnetic interaction can be estimated[22] from eq 2:

$$g\mu_B SH_C = 2|zJ'|S^2 \quad (2)$$

where z is the number of near-neighbor chains. By assuming that $H_c = 0.05$ T, $g = 2.292$, and $S = 2$, an interchain magnetic interaction, $|zJ'|/k_B$, value of 0.02 K is obtained. With $z = 2$, $J' = 0.01$ K can then be used to estimate[23] the ordering temperature, T_c, from eq 3:

$$k_B T_C = 4S(S+1)|J_I J|^{1/2} \quad (3)$$

which yields a T_c of 2.15 K, a value that is in agreement with the critical temperatures obtained from the dc and ac susceptibility measurements, see above and below. The

hysteresis loop of **1** obtained at 1.8 K is shown in Figure 5. This hysteresis loop covers a narrow ±0.023 T field range and exhibits a coercive field of 8.7×10^{-3} T.

The metamagnetic behavior of **1** has also been observed in the zero-field and field-cooled susceptibility measurements, see Figure 6. In a small external field of 0.001 T, see the inset to Figure 6, an irreversible change is observed at 2.5 K, as indicated by the difference between the zero-field and field-cooled magnetizations below 2.5 K. However, both magnetization curves exhibit a cusp at 2.5 K, a cusp that suggests the presence of long-range antiferromagnetic order. When the field is increased from 0.001 to 0.1 T, the difference between the zero-field and field-cooled magnetization disappears, at least above 1.8 K. Such a difference is usually observed in time-dependent dynamic magnetic systems, such as spin-glasses or superparamagnets, at the onset of their slow-relaxation or "blocked" regime.[24,25]

To further investigate the magnetic behavior of **1**, the temperature dependence of the ac susceptibility was measured in a 0 and 0.1 T applied dc field. In a zero dc field, see Figure 7, both the real, χ', and imaginary, χ'', ac susceptibility components show a cusp at 2.5 K; no frequency-dependent behavior is observed for χ' between 10 and 1000 Hz, whereas χ'' exhibits a small increase with increasing frequency. Further, the maximum in $\chi''(T)$ is 2 orders of magnitude smaller than that for $\chi'(T)$. The presence of a cusp in the temperature dependence of both χ' and χ'' indicates that long-range magnetic order occurs below 2.5 K. Further, the small χ'' value possibly indicates weak ferromagnetism induced by spin-canting in **1**. In contrast, in a 0.1 T dc field, see Figure 8, both $\chi'(T)$ and $\chi''(T)$ exhibit a strong frequency-dependent behavior; the maximum value of $\chi''(T)$ increases by a factor of ca. 100 as compared to the zero-field value, see Figure 7. If T_P is the temperature of the maximum in χ' and f is the frequency of the ac field, the frequency dependence of T_P is given by $\varphi = (\Delta T_p/T_p)/\Delta(\log f)$.[25] In **1**, φ is greater than 0.10, a value that indicates a superparamagnetic-like behavior rather than a spin-glass behavior.[25]

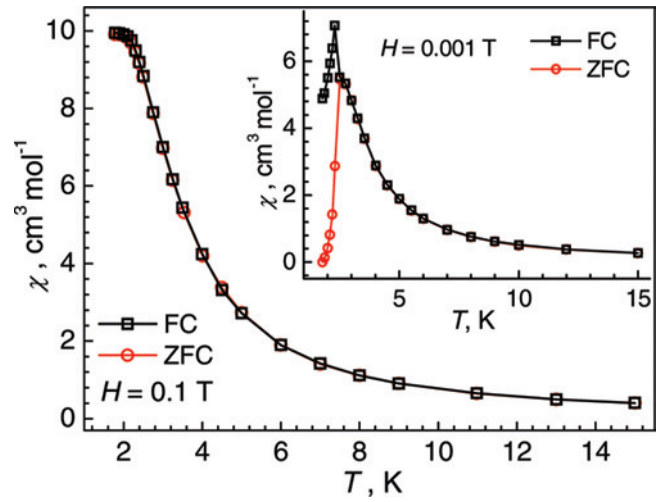

Figure 6. The temperature dependence of the zero-field and field-cooled susceptibility measured on a powder sample of **1** in an applied field of 0.1 T. Inset: The analogous susceptibilities obtained in a 0.001 T applied field.

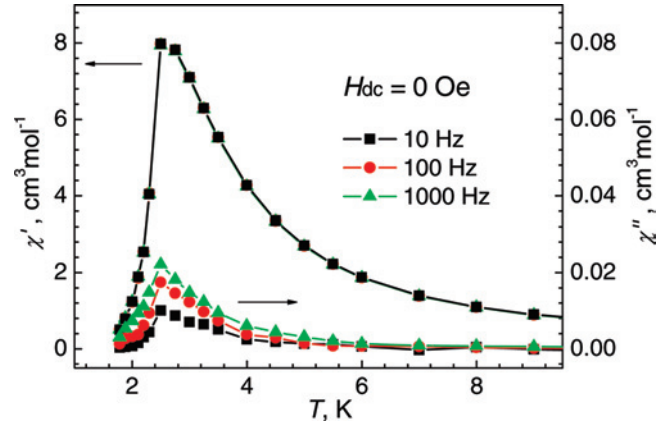

Figure 7. The temperature dependence of the real, χ', and imaginary, χ'', components of the ac susceptibility of **1** obtained in a zero-applied dc field at the indicated frequencies. It should be noted that all of the χ' values for the three frequencies are coincident.

The relaxation time, τ, of superparamagnetic particles may be obtained from the expression, $2\pi f\tau = 1$, and the temperature dependence of τ should follow an Arrhenius law, $\tau = \tau_0 \exp(\Delta_\tau/k_B T)$. A fit of the temperature maximum observed for $\chi''(T)$ at 500, 750, 1000, 1250, and 1500 Hz with this Arrhenius law yields $\tau_0 = 4.0 \times 10^{-10}$ s and $\Delta_\tau =$ 24.8(8) K. However, these values must be considered with caution because of the very narrow 1.8−2 K temperature range covered by the measurements. Thus, to verify these results, we have also fit the frequency dependence of the ac susceptibility measured between 1.8 and 2.1 K with a generalized Debye model, see Figure S4 of the Supporting Information. The resulting relaxation times obey the Arrhenius law, see Figure S5 of the Supporting Information, and yield $\tau_0 = 7.0 \times 10^{-9}$ s and $\Delta_\tau = 20.0(2)$ K. Although these values are somewhat different, they are consistent with the above values, and we estimate that Δ_τ is 23(3) K. Moreover, as expected for particles or chain segments relaxing with a distribution of relaxation times, the plots of χ'' versus χ', see Figure 9, approach the semicircular Cole–Cole dia-

(21) (a) Qin, C.; Wang, X.-L.; Li, Y.-G.; Wang, E.-B.; Su, Z.-M.; Xu, L.; Clérac, R. *Dalton Trans.* **2005**, 2609–2614. (b) Mukherjee, P. S.; Konar, S.; Zangrando, E.; Mallah, T.; Ribas, J.; Chaudhuri, N. R. *Inorg. Chem.* **2003**, *42*, 2695–2703. (c) Du, M.; Bu, X.-H.; Guo, Y.-M.; Zhang, L.; Liao, D.-Z.; Ribas, J. *Chem. Commun.* **2002**, 1478–1479. (d) Costa-Filho, A. J.; Nascimento, O. R.; Ghivelder, L.; Calvo, R. *J. Phys. Chem. B* **2001**, *105*, 5039–5047. (e) Sanchiz, J.; Rodruez-Martín, Y.; Ruiz-Pérez, C.; Mederos, A.; Lloret, F.; Julve, M. *New J. Chem.* **2002**, *26*, 1624–1628.

(22) Chikazumi, S. *Physics of Ferromagnetism*; Clarendon Press Oxford Science Publications: Oxford, 1997; p 521.

(23) (a) Richards, P. M. *Phys. Rev. B: Condens. Matter Mater. Phys.* **1974**, *10*, 4687–4689. (b) Panissod, P; Drillon, M. In *Magnetism: Molecules to Materials*; Miller, J. S.; Drillon, M., Eds.; Wiley-VCH Verlag: Berlin, 2001; Vol. IV, pp. 234–270.

(24) (a) Tejada, J.; Zhang, X. X.; Chudnovsky, E. M. *Phys. Rev. B: Condens. Matter Mater. Phys.* **1993**, *47*, 14977–14987. (b) Tejada, J.; Ziolo, R. F.; Zhang, X. X. *Chem. Mater.* **1996**, *8*, 1784–1792. (c) Barco, E.; del Asenjo, J.; Zhang, X. X.; Pieczynski, R.; Julià, A.; Tejada, J.; Ziolo, R. F.; Fiorani, D.; Testa, A. M. *Chem. Mater.* **2001**, *13*, 1487–1490.

(25) (a) Ma, S. K. *Phys. Rev. B: Condens. Matter Mater. Phys.* **1980**, *22*, 4484–4502. (b) Mydosh, J. A. *Spin Glasses: An Experimental Introduction*; Taylor & Francis: London, 1993.

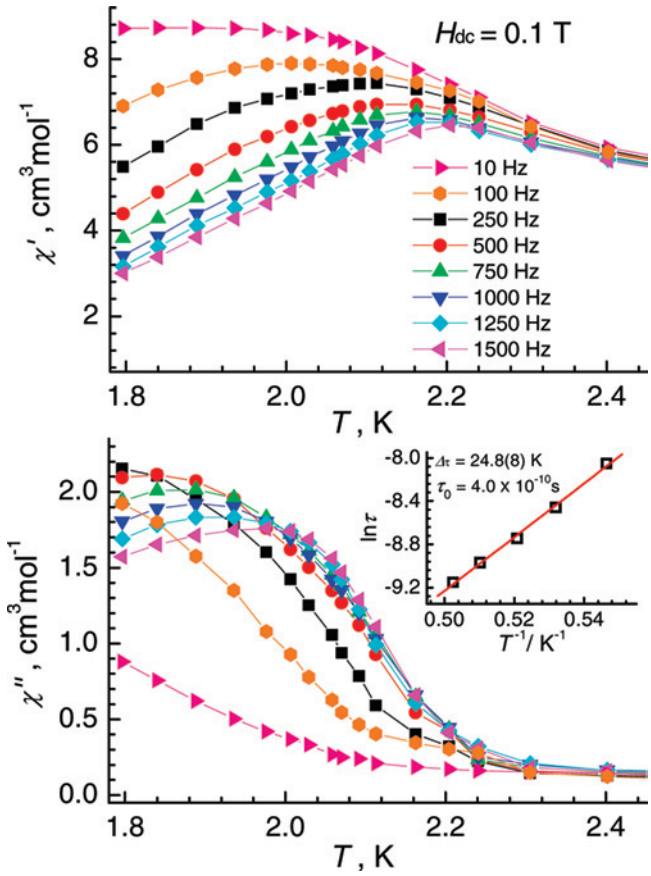

Figure 8. The temperature dependence of the real, χ', upper plot, and imaginary, χ'', lower plot, components of the ac susceptibility of **1** measured in an applied dc field of 0.1 T. Inset: The logarithm of the relaxation time versus $1/T$. The red line is the result of an Arrhenius least-squares fit.

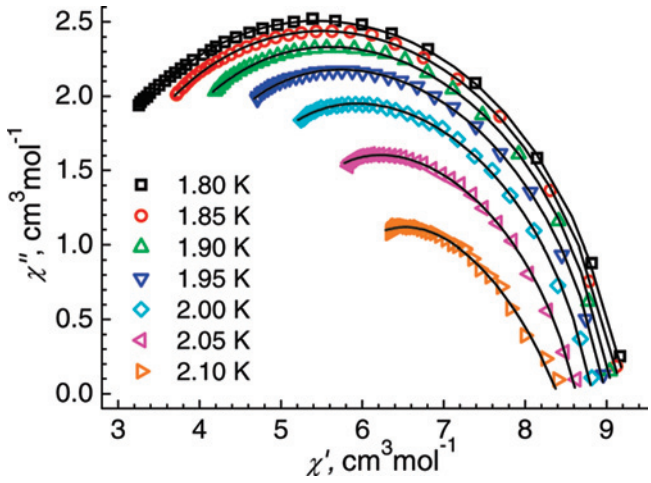

Figure 9. The Cole–Cole diagram of **1** obtained at the indicated temperatures. The measurements have been obtained in an applied dc field of 0.1 T between 1 and 1500 Hz. The lines are the results of fits with the generalized Debye model.

grams.[26] Their fit, see Figure 9, with eqs S1 and S2, given in the Supporting Information, yields α values between 0.26 and 0.33, values that correspond to a narrow distribution of relaxation times.

Rationalization of the Metamagnetic Behavior. The metamagnetism and the field-assisted slow-relaxation in **1** are very interesting and unexpected properties that need to be understood. According to recent studies of some iron(II)-based molecular magnets,[27] the sign of the zero-field-splitting parameter, D, for an axially elongated octahedral iron(II) ion, can be either positive, in the case of an easy-plane anisotropy, or negative, in the case of an easy-axis anisotropy. If the equatorial donors exhibit π character, D tends to be positive, whereas if the equatorial donors exhibit σ character, D tends to be negative.[2g,27,28] Because the equatorial carboxylato-O donors exhibit σ character, D may be assumed to be negative. Hence, easy-axis anisotropy is expected for **1** with the principal axis of the iron(II) easy-anisotropy tensor coincident with the linear N−Fe−N Jahn–Teller axis.

Because all of the intrachain Jahn–Teller axes, the easy magnetic axes, are parallel in **1**, all of the spins are collinear within a given iron(II)−carboxylate chain. However, because of the angle between the Jahn–Teller axes, the spins on adjacent chains are not collinear. Therefore, as is illustrated in Scheme 2, when the applied field, H, is less than the critical field, H_c, the resulting small net magnetization is parallel with the b axis. As shown in Figure 1a and b, this spin arrangement leads to two-dimensional ordered layers in the bc plane. Because of the absence of interlayer bonding, adjacent layers interact with each other mainly through rather weak dipole–dipole interactions. These weak interactions will exclude the possibility of any strong antiferromagnetic or ferromagnetic exchange coupling interactions between the layers, coupling that could lead to three-dimensional magnetic ordering.[29]

When the external field is increased, the tendency of the spins to align parallel with the field competes with the interchain antiferromagnetic interaction. Above a critical applied field of 0.05(2) T, the interchain antiferromagnetic interactions in **1** are fully overcome by the external field. It should be noted that the external field does not transform **1** into a three-dimensionally ordered ferromagnetic phase but just overcomes the antiferromagnetic interaction between the chains, such that the spins within a chain may "freely" rotate. Accordingly, the slow-relaxation behavior of **1** in an appropriate applied field should yield an Ising-type ferromagnetic spin-chain that cannot be easily reversed. Because of the angle between the Jahn–Teller axes, that is, the spin directions, the interchain Ising spins are not parallel with

(26) Cole, K. S.; Cole, R. H. *J. Chem. Phys.* **1941**, *9*, 341–351.

(27) (a) Oshio, H.; Hoshino, N.; Ito, T.; Nakano, M. *J. Am. Chem. Soc.* **2004**, *126*, 8805–8812. (b) Oshio, H.; Hoshino, N.; Ito, T. *J. Am. Chem. Soc.* **2000**, *122*, 12602–12603. (c) Oshio, H.; Nakano, M. *Chem.—Eur. J.* **2005**, *11*, 5178–5185. (d) Boudalis, A. K.; Donnadieu, B.; Nastopoulos, V.; Clemente-Juan, J. M.; Mari, A.; Sanakis, Y.; Tuchagues, J.-P.; Perlepes, S. P. *Angew. Chem., Int. Ed.* **2004**, *43*, 2266–2270. (e) Boudalis, A. K.; Sanakis, Y.; Clemente-Juan, J. M.; Mari, A.; Tuchagues, J.-P. *Eur. J. Inorg. Chem.* **2007**, 2409–2415.

(28) (a) Figgis, B.; Hitchman, M. A. *Ligand Field Theory and its Applications*; Wiley-VCH: New York, 2000. (b) Solomon, E. I.; Lever, A. B. P. *Inorganic Electronic Structure and Spectroscopy*; John Wiley & Sons: New York, 1999; Vol. 1: Methodology.

(29) Rabu, P.; Drillon, M.; Awaga, K.; Fujita, W.; Sekine, T. *Hybrid Organic-Inorganic Multilayer Compounds: Towards Controllable and/or Switchable Magnets in Magnetism: Molecules to Materials*; Miller, J. S., Drillon, M., Eds.; Wiley-VCH: Weinheim, Germany, 2002; Vol. II, pp. 357–395.

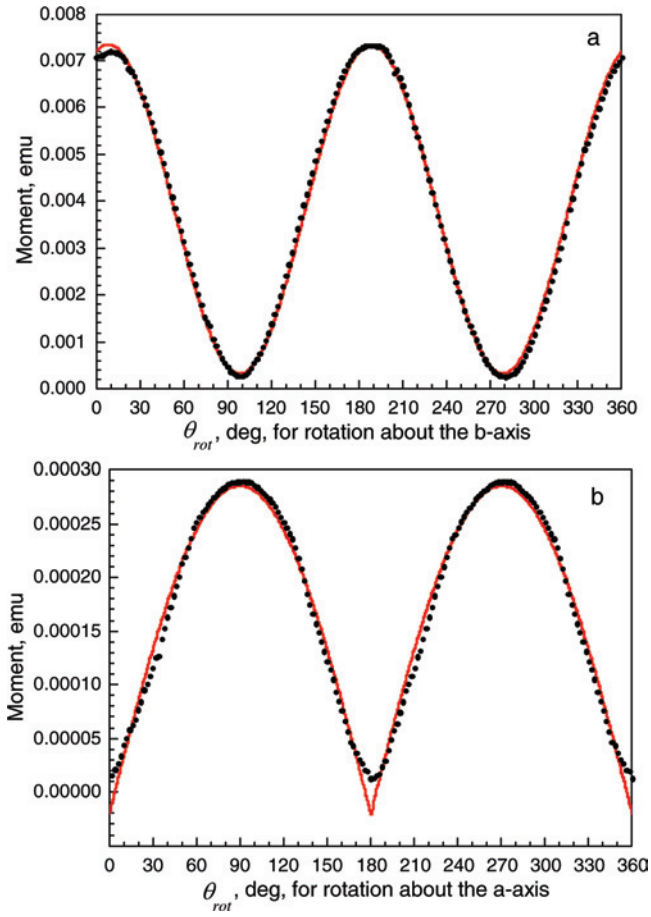

Figure 10. The 4.2 K dependence of the magnetic moment upon rotation about the *b* axis (a) and the *a* axis (b) of a single crystal of **1** in an applied dc field of 0.1 T. The red lines correspond to fits with eqs 4 and 5 in the text.

the external field. The maximum projection of the magnetization is observed along the direction of the bisector of the Jahn–Teller axes, that is, the *a* axis.

The quasi-uniaxial magnetic anisotropy of **1** has been confirmed by magnetic measurements on an oriented single crystal. The magnetic moment measured upon rotation of a single crystal of **1** about two different axes is shown in Figure 10. For a rotation about the *b* axis and *a* axis, $\theta_{rot} = 0°$ corresponds to a magnetic field of 0.1 T applied parallel to the *a* axis and the *b* axis, respectively. Unfortunately, it is very difficult inside the magnetometer to accurately orient the small single crystal, see Figure S2 in the Supporting Information, in the applied field, and an error, θ_{cor}, of several degrees in the $\theta_{rot} = 0°$ orientation is possible. For rotation about the *b* axis, an oscillatory behavior of the magnetic moment, see Figure 10a, is observed with maxima at ca. 8 and 188°, an oscillation that can be fit with eq 4:

$$M = M_s \times \cos^2(\theta_{rot} - \varphi + \theta_{cor}) + k = (M_s/2) \times \cos[2(\theta_{rot} - \varphi + \theta_{cor})] + k \quad (4)$$

with $M_s = 0.00702$ emu, $\varphi = 24.24°$, $\theta_{cor} = 15.86°$, and $k = 0.00033$ emu. The maxima in the magnetic moment are expected to occur for θ_{rot} values corresponding to $\varphi = 24.24°$, the angle between the projection of the two Jahn–Teller axes onto the *ac* plane and the *a* axis. Hence, we are forced to

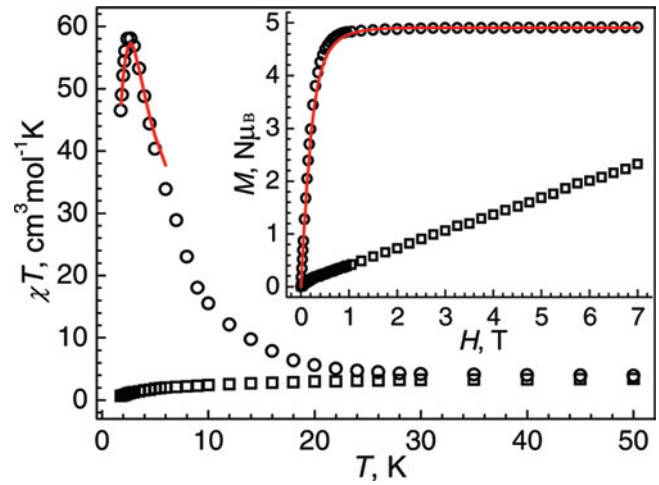

Figure 11. The temperature dependence of the field-cooled χT obtained on a single crystal of **1** in a field of 0.1 T applied parallel to the *a* axis, circles, and parallel to the *b* axis, squares. Inset: The field dependence of the magnetization measured at 4.2 K. The red lines result from a fit with the one-dimensional Ising model.

conclude that the $\theta_{rot} = 0°$ orientation of the single crystal was off by $\theta_{cor} = 15.86°$.

For rotation about the *a* axis, a different oscillatory behavior of the magnetic moment, see Figure 10b, is observed, with much smaller, more-rounded, maxima at ca. 90 and 270°, and much sharper minima at 0 and 180°, a behavior that can be fit with eq 5:

$$M = |M_s \times \sin(\theta_{rot})| + k \quad (5)$$

with $M_S = 0.00031$ emu and $k = -0.00002$ emu. These maxima are much smaller than those observed in Figure 10a because the magnetic moment is measured in the magnetic hard *bc* plane. The maxima are observed for θ_{rot} values that correspond to the applied field virtually along the *c* axis, in agreement with the angle of 64.515° between the Jahn–Teller axes and the *c* axis, versus the angle of 81.04° between the Jahn–Teller axes and the *b* axis because the cosine of 64.515° is larger than that of 81.04°. Finally, no θ_{cor} is needed in eq 5, and hence, for the rotation about the *a* axis, the orientation of the *b* axis of the single crystal parallel with the applied field was virtually perfect. This better orientation surely results from the shape of the single crystal, shown in Figure S2 in the Supporting Information, a crystal that has a long *b* axis and a very short, 0.125 mm, *a* axis. The observed angular dependence of the moment about the *a* axis indicates the presence of a magnetic anisotropy in the *bc* plane, the hard magnetic anisotropy plane, an anisotropy that is also observed in the single-crystal magnetization studies reported below.

Magnetic measurements on a single crystal of **1** have also been performed with the applied field along both the *a* and *b* axes, see Figure 11. The magnetization is significantly anisotropic below ca. 20 K, and the 4.2 K field dependence of the magnetization along the *a* axis, see inset to Figure 11, saturates at 4.91 μ_B per iron(II) at a field of ca. 0.7 T, a saturation that indicates that the *a* axis is the easy axis of magnetization. An extrapolation of the magnetization measured parallel to the *b* axis to that measured parallel with the *a* axis yields an anisotropy field, H_a, of ca. 14 T at 4.2 K.

To model the magnetic results shown in Figure 11, the simplest approach is the one-dimensional Ising model for $S = 2$. The corresponding Hamiltonian can be written[1,2b,4] as

$$\hat{H} = -J_{\text{eff}}S^2 \sum_{i=1}^{N} \sigma_i\sigma_{i+1} + g_z\mu_B HS \sum_{i=1}^{N} \sigma_i \qquad (6)$$

where J_{eff} is the effective intrachain magnetic interaction and σ_i is a unit vector. This model yields[1,2b,4] eq 7, the magnetization as a function of temperature and magnetic field:

$$m = \frac{\sinh(\mu_{\text{eff}}H/k_BT)}{\sqrt{\sinh^2(\mu_{\text{eff}}H/k_BT) + \exp(-4J_{\text{eff}}/k_BT)}} \qquad (7)$$

where μ_{eff} is g_zS in μ_B. The red lines in Figure 11 are the result of a fit between 1.8 and 7 K using eq 7 with $g_z = 2.45(4)$, $\mu_{\text{eff}} = 2g_z\mu_B = 4.91(7)\ \mu_B$, and $J_{\text{eff}}/k_B = 2.06(8)$ K; the fit has a reliability, R, of 3.6×10^{-4}. This satisfactory fit confirms that both the peak in χT and the rapid saturation of the magnetization along the a axis are compatible with one-dimensional Ising behavior along the chain, that is, the peak in χT does not result from long-range magnetic order.

Further single-crystal magnetic studies of **1** between 1.8 and 15 K in a field of 0.01−0.5 T applied along the a axis also confirm the presence of field-induced metamagnetic behavior, see Figure S6 in the Supporting Information, behavior that is similar to that observed for the powder sample. This study reveals both that the a axis is not the easy axis of the bulk material at applied fields smaller than 0.1 T and that the spins reverse as the field is increased above 0.1 T, in agreement with Scheme 2. The spin reversal is also confirmed by the $M(H)$ loop observed with the field applied along the a axis at 1.8 K, see Figure S7 in the Supporting Information, a loop that is similar to, but having a smaller area than, that obtained on the powder sample, see Figure 5. The loop is open between ±0.022 T fields that are below the critical field, and at 1.8 K, **1** exhibits a coercive field of 0.004 T, a value that is smaller than the 0.01 T coercive field found for the powder. This result is reasonable because, below the critical field, the net moment of the canted spins is along the b axis and thus is perpendicular to the a axis, see Scheme 2. Hence, the a axis can be regarded as the "hard axis," but only when the applied field is smaller than the critical field.

Dynamics of the Field-Assisted Single-Chain Magnetic Behavior. According to the Glauber model, eq 6 in ref 1, χ diverges[1] exponentially as

$$\chi T = C_{\text{eff}} \exp(\Delta_\xi/k_BT) \qquad (8)$$

Therefore, the low-energy excited states of an Ising chain consist of oriented domains separated by sharp domain walls, a separation that is totally different from the gapless energy excited states of a Heisenberg chain, see eq 1 above. In the Glauber model, the energy barrier for creating a domain wall, Δ_ξ, is equal to $4J_{\text{eff}}/k_B = 8.2(2)$ K for **1**. Alternatively, Δ_ξ can be obtained from a linear least-squares fit of $\ln(\chi T)$ versus T^{-1}; the red line in Figure 12 is the result of such a fit between 0.02 and 0.2 K^{-1}, that is, between 40 and 5 K, and

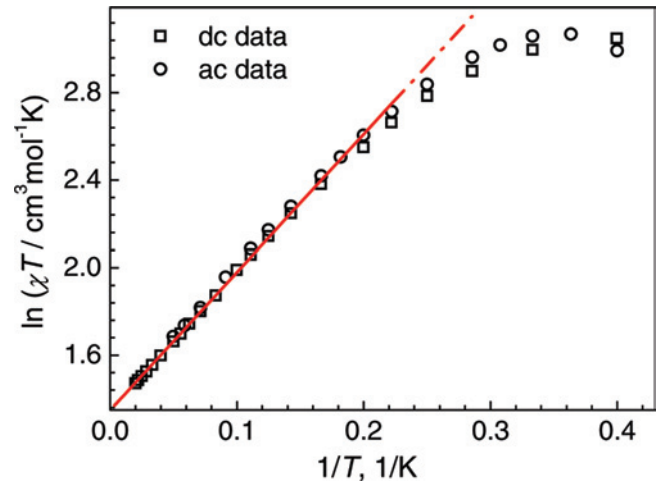

Figure 12. The logarithm of χT vs $1/T$. The ac susceptibility was obtained at a frequency of 10 Hz in an ac field of 5×10^{-4} T. The dc susceptibility was obtained in an applied field of 0.1 T, see inset to Figure 3. The red line is the result of a fit between 5 and 40 K.

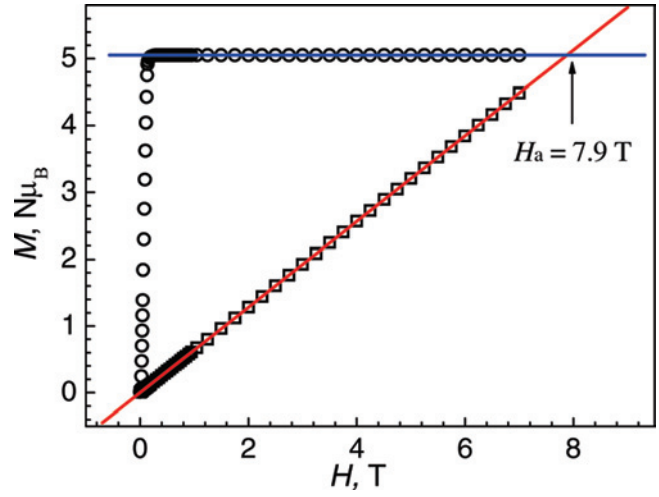

Figure 13. The 1.8 K field dependence of the magnetization of a single crystal of **1** measured with the field applied parallel to the a axis, circles, and parallel to the c axis, squares. The solid lines result from linear fits, and their intersection yields the anisotropy field, H_a.

the slope yields a Δ_ξ of 6.3(1) K, a value that is consistent with the above 8.2(2) K value. Further, the $\ln(\chi T)$ versus T^{-1} curve saturates at the lowest temperatures, that is, below ca. 5 K, because of finite size effects.[1] However, for an infinite chain with substantial anisotropy, the relaxation time, τ, of the magnetization has a gap activation energy given by $\Delta_\tau = 2\Delta_\xi + \Delta_A$, where Δ_A is the activation energy resulting from the single-ion anisotropy, that is, $\Delta_A = |D|S^2$, an energy which, in turn, depends on the single-ion anisotropy constant, D, of the iron(II) ion.

In order to obtain an estimate of the iron(II) single-ion anisotropy, D, single-crystal magnetic measurements at the lowest possible temperature are necessary. The field dependence of the magnetization was measured at 1.8 K, with the field applied parallel to both the a axis and c axis, see Figure 13. As is shown by the squares in Figure 13, the magnetization along the c axis does not reach saturation even at 7 T. However, it increases linearly with the applied field, and an extrapolation of the a and c axis magnetizations yields an anisotropy field, H_a, of 7.9 T.

A comparison of Figures 11 and 13 is useful because, along the *b* axis, see the inset to Figure 11, $H_a = \sim 14$ T at 4.2 K, an anisotropy field that is almost twice as large as the $H_a = 7.9$ T field obtained at 1.8 K along the *c* axis, see Figure 13. Because the anisotropy fields should be almost the same at 4.2 and 1.8 K, one may conclude that, for $H > H_c$, the *a* axis is the easy axis, the *b* axis is the hard axis, and the *c* axis is the intermediate axis of magnetization in **1**. Further, the *ac* plane is the easy plane, the *bc* plane is the hard plane, and the *ab* plane is the intermediate plane of magnetization in **1**. The difference between the anisotropy fields of 7.9 and 14 T results from the anisotropy in the *bc* plane, an anisotropy that is somewhat different than the several examples discussed by Coulon et al.[1]

If the H_a field of ca. 7.9 T from Figure 13 is used to estimate the iron(II) single-ion anisotropy constant, *D*, from eq 9

$$2|D|S^2 = g\mu_B H_a S \tag{9}$$

then a $|D|/k_B$ value of 3.2(1) K is obtained, a value which is reasonable for a high-spin iron(II) ion.[6b,27,28,30] This value corresponds to $\Delta_A = 12.8(4)$ K and leads to $\Delta_\xi' = (\Delta_\tau - \Delta_A)/2 = 5.0(1.6)$ K, if one uses $\Delta_\tau = 23(3)$ K as has been obtained above. This Δ_ξ' value agrees reasonably well with the experimental value of $\Delta_\xi = 6.3(1)$ K obtained above.[31] This result qualifies **1** as an "Ising-limit" complex because $|D|/J_{eff} > 4/3$, which indicates that its large oriented domains are separated by sharp domain walls, in agreement with the parallel arrangement of the Jahn–Teller axes in a given chain, and suggests that the field-assisted slow-relaxation behavior of **1** observed by ac susceptibility is consistent with the dynamics of a single-chain magnet and that **1** may qualify as a "metamagnetic-like" single-chain magnet.[9a,b] In contrast, if the anisotropy field of ca. 14 T obtained from Figure 11 is used in eq 9, a $|D|/k_B$ value of 5.7(2) K is obtained and yields $\Delta_A = 22.7(2)$ K, a value that is very close to Δ_τ. This leads to a nearly zero value of Δ_ξ and would indicate that the dynamics of **1** result predominately from the iron(II) single-ion anisotropy rather than from the single-chain magnetic structure. We believe that this result is incompatible with the behavior observed in Figure 12, a behavior that is typical[1] of a single-chain magnet.

Conclusions

A two-dimensional layered polymer, $[Fe(pyoa)_2]_\infty$, containing chains of pseudooctahedral high-spin iron(II) ions linked by syn−anti μ-carboxylates has been synthesized. This polymer exhibits field-induced metamagnetic behavior such that, below a critical field, the iron(II) spin-canted moments experience intrachain ferromagnetic interactions and weak interchain antiferromagnetic interactions; the combination of these interactions leads to weak ferromagnetism. Above the critical field, the weak antiferromagnetic interchain interactions are overwhelmed to yield superparamagnetic-like slow-magnetic relaxation with an energy barrier of 23(3) K, relaxation that is characteristic of single-chain magnet behavior. This unprecedented field-induced transition from long-range magnetic order to single-chain magnetic behavior suggests that classical to nonclassical magnetic behavior can be controlled not only by structural diversity but also by an external stimulus, such as an applied magnetic field. Such a simple external control may find future technological applications.

Acknowledgment. The authors thank one of the referees for providing a very helpful review. This work was supported by the "973 Project" (2007CB815302), NSFC (No. 20531070) and Science and Technology Department of Guangdong Province (No. 04205405) and by the National Fund for Scientific Research, Belgium, grant 1.5.064.05.

Supporting Information Available: CIF files, additional structural plots, additional magnetic data, and the X-ray diffraction patterns are available at http://pubs.acs.org.

IC701879Y

(30) (a) Goldberg, D. P.; Telser, J.; Bastos, C. M.; Lippard, S. J. *Inorg. Chem.* **1995**, *34*, 3011–3024. (b) Feig, A. L.; Lippard, S. J. *Chem. Rev.* **1994**, *94*, 759–805. (c) Sun, J.-S.; Zhao, H.; Ouyang, X.; Clérac, R.; Smith, J. A.; Clemente-Juan, J. M.; Gómez-Garcia, C.; Coronado, E.; Dunbar, K. R. *Inorg. Chem.* **1999**, *38*, 5841–5855. (d) Knapp, M. J.; Krzystek, J.; Brunel, L.-C.; Hendrickson, D. N. *Inorg. Chem.* **2000**, *39*, 281–288. (e) Davydov, R.; Perera, R.; Jin, S.; Yang, T.-C.; Bryson, T. A.; Sono, M.; Dawson, J. H.; Hoffman, B. M. *J. Am. Chem. Soc.* **2005**, *125*, 1403–1413. (f) Solomon, E. I.; Brunold, T. C.; Davis, M. I.; Kemsley, J. N.; Lee, S.-K.; Lehnert, N.; Neese, F.; Skulan, A. J.; Yang, Y.-S.; Zhou, J. *Chem. Rev.* **2000**, *100*, 235–349.

(31) (a) Coulon, C.; Clérac, R.; Lecren, L.; Wernsdorfer, W.; Miyasaka, H. *Phys. Rev. B: Condens. Matter Mater. Phys.* **2004**, *69*, 132408/1–4. (b) Bogani, L.; Caneschi, A.; Fedi, M.; Gatteschi, D.; Massi, M.; Novak, M. A.; Pini, M. G.; Rettori, A.; Sessoli, R.; Vindigni, A. *Phys. Rev. Lett.* **2004**, *92*, 207204/1–4. (c) Bogani, L.; Sessoli, R.; Pini, M. G.; Rettori, A.; Novak, M. A.; Rosa, P.; Massi, M.; Fedi, M. E.; Giuntini, L.; Caneschi, A.; Gatteschi, D. *Phys. Rev. B: Condens. Matter Mater. Phys.* **2005**, *72*, 064406/1–10.